Journal of Ceramic Processing Research. Vol. 21, No. 2, pp. 233~239 (2020)
(Received 2 December 2019, Received in revised form 28 December 2019, Accepted 2 January 2020)
https://doi.org/10.36410/jcpr.2020.21.2.233

J O U R N A L O F
Ceramic Processing Research

Piezoelectric parameters and impedance analysis of sol gel processed Ce-doped $BaTi_{0.97}Y_{0.03}O_3$ ceramics

Aziz Nfissi[a], Yahya Ababou[a], Salaheddine Sayouri[a,*], Lamiae Mrharrab[a,b], Fouzia Saadaoui[a], Elmaati Ech-chamikh[c] and Taj-dine Lamcharfi[d]
[a]*LPTA, Faculty of Sciences-DM, USMBA, B.P. 1796, Fez-Atlas, Morocco*
[b]*ERMAM, FP, Ouarzazate, Morocco*
[c]*LNEE, Faculty of Sciences Semlalia, Cadi Ayad University, BP. 2390, Marrakesh, Morocco*
[d]*LSSC, FST-Fès, Route d'Imouzzer, B.P. 2202, Fès, Morocco*

A series of Ce-doped $BaTi_{0.97}Y_{0.03}O_3$ powder samples with the composition $(Ba_{1-x}Ce_x)(Ti_{(0.97-x/4)}Y_{0.03})O_3$ (x = 0.00, 0.01, 0.03, 0.05, 0.07 and 0.09) were prepared using the sol gel process and calcined at a relatively low temperature (950°C/4h) and their structural and piezoelectric properties investigated. From structural investigations, it was observed that the samples crystallize in the pseudo cubic phase with the presence of secondary phases for concentrations such as x > 0.03. Piezoelectric parameters were determined and their thermal behavior investigated. The impedance study indicated the dominance of the resistance of the grain boundaries compared to that of grains in $BaTi_{0.97}Y_{0.03}O_3$ sample.

Keywords: Sol gel process, Ce-doped $BaTi_{0.97}Y_{0.03}O_3$, Piezoelectric properties, Complex impedance.

Introduction

Barium Titanate ($BaTiO_3$), with a perovskite structure of a general formula ABO_3, is one of the ceramic materials that exhibit interesting ferroelectric, dielectric and piezoelectric properties with wide technological applications such as ultrasonic transducers, Multilayer Ceramic (MLCCs), detection of gaseous pollutants like CO, ferroelectric random access memories (FRAM's), Positive temperature coefficient resistors (PTCR), pyroelectric security surveillance systems, IR detectors, etc. [1-5]. Ferroelectric materials form a sub-group of piezoelectric materials. In ABO_3 perovskite materials, piezoelectric properties have been shown to be improved under particular conditions such as near phase transitions [6] or with compositions of ceramics close to the morphotropic phase boundary [7]. Attempts have also been made to enhance these properties through doping [8-14]. Doping $BaTiO_3$ with rare earth elements was shown to improve its permittivity and to give rise to excellent electrical properties [15]. In particular, it was observed that incorporation of most of RE elements in $BaTiO_3$ matrix lowered the temperature of the ferro-to-paraelctric phase transition (Curie point) [16], and that these RE elements may occupy Ba or/ and Ti sites depending on their ionic radii. However, the procedure of synthesis has a great influence on this sites occupation property [17, 18]. In ABO_3 structured compounds, A ion is twelve fold coordinated by oxygen ions and B ion is octahedrally coordinated by oxygen ions. The origin of ferroelectricity in $BaTiO_3$ derives from the displacement of ions relative to each other. $BaTiO_3$ is a ferroelectric material of which dielectric properties can be modified by chemical substitution of barium and/or titanium by a wide variety of isovalent and aliovalent dopants. In addition to the sintering process, these properties are however greatly influenced by impurities, especially by a donor or an acceptor dopant. It is also known that cerium, which is a donor dopant, occupies the Ba sites in the crystal lattice of $BaTiO_3$. On the other hand, substitution of Ce^{3+} on Ba^{2+} sites creates charge defects. Doping with Ce have been reported to influence the piezoelectric response of the doped material ($BaTiO_3$). Brajesh et al. [19] elaborated Ba(Ti, Ce)O_3 samples (Ce^{3+} substitutes Ti^{4+} ions in $BaTiO_3$ matrix) and have observed that the (longitudinal) piezoelectric charge coefficient (d_{33}) increased first, reached its maximum value at 2% in Ce before it decreased.

The aim of the present work is the synthesis, by the sol gel process, and the characterization of $BaTi_{0.97}Y_{0.03}O_3$ and cerium doped $BaTi_{0.97}Y_{0.03}O_3$ materials, in view of investigation of the influence of doping $BaTiO_3$ material with Ce^{3+} ions at Ba sites on their piezoelectric properties.

*Corresponding author:
Tel : +212 6 73 78 52 88
Fax: +212 535 73 33 49
E-mail: ssayouri@gmail.com

Experiment

The following precursors were needed to synthesize the series of samples $(Ba_{1-x}Ce_x)(Ti_{(0.97-x/4)}Y_{0.03})O_3$ (BCYTx): barium acetate trihydrate ($Ba(CH_3COO)_2$, $3H_2O$), titanium isopropropoxide $Ti[OCH(CH_3)_2]_4$, yttrium (III) acetate hydrate ($Y(C_6H_9O_6)$,H_2O) and Cerium(III) acetate hydrate ($Ce(CH_3COO)_3$,H_2O). During the preparation process, lactic acid ($C_3H_6O_3$) was used as peptizing agent. Calcination in air of the raw powders was done in a programmable oven at the temperature of 950 °C for 4 h. For dielectric measurements, uniaxially pressed pellets (of around 1.2 mm thickness and a diameter of around 12 mm) were sintered at 1200 °C for 6 h in a programmable oven. The structural properties of the samples were investigated using an X-ray diffraction diffractometer (XPERT-PRO) with Cu-Kα radiation (λ = 1.54059 Å). The dielectric measurements were carried out in the frequency range 1 kHz to 2 MHz and temperature from ambient to 380 °C using an Agilent 4284A precision impedance analyzer (Hewlett-Packard, Palo Alto, CA).

Results and Discussion

Structural analysis

The room temperature X-ray diffraction (XRD) patterns of the as-prepared $(Ba_{1-x}Ce_x)(Ti_{(0.97-x/4)}Y_{0.03})O_3$ samples (BCYTx, x = 0; 1; 3; 5; 7 and 9%), calcined at 950 ºC-4 h (Fig. 1), revealed well resolved peaks corresponding to the pseudo cubic structure with the presence of $BaCeO_3$ secondary phase (detected at 28.5°) at concentrations in Ce such as x > 0.03.

Table 1 gathers the values of the lattice parameters (a, c), the tetragonality (c/a) and the unit cell volume (V) of BCYTx. A substitution of Ba^{2+} ions by Ce^{3+} ones in $BaTi_{0.97}Y_{0.03}O_3$ matrix results in a shrinkage of the volume of the unit cell until 7% in Ce^{3+}, because the ionic radius of Ce^{3+}($r(Ce^{3+})$ = 1.34 Å, coordination number (CN) = 12) is smaller than that of Ba^{2+}($r(Ba^{2+})$ = 1.61 Å, CN = 12). Therefore, an expansion of this volume for the concentration x > 0.07 can be ascribed to the occupation of Ce^{3+} ions of Ti-sites as the ionic radius of Ce^{3+}($r(Ce^{3+})$ = 1.01 Å, CN = 6) is larger than that of Ti^{4+}($r(Ti^{4+})$ = 0.605 Å, CN = 6).

Moreover, doping with Ce gave rise to a shift of the position of the XRD peaks to high values (x < 0.07) (Fig. 1), which reveals a shrinkage of the unit cell (as indicated by the Bragg relation $2d\sin(\theta) = n\lambda$), and, consequently, a reduction of its volume as illustrated on Fig. 2 displaying the evolutions of the position of the peak (110) and the volume of the unit cell, in conformity with the discussion of the site occupation of Ba given above.

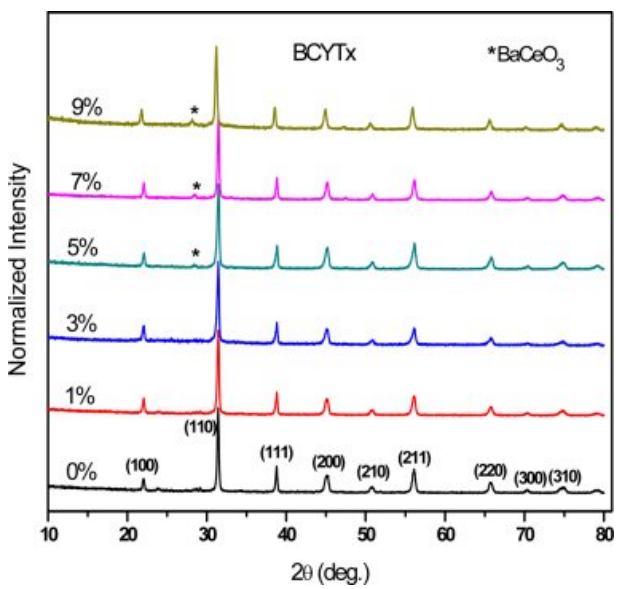

Fig. 1. XRD patterns of BCYTx samples.

Piezoelectric studies

The piezoelectric coefficients were determined using the resonance and anti-resonance frequencies obtained from the variation of the dielectric permittivity with frequency, for each temperature [20], of the BCYTx samples (x = 0; 3; 7 and 9%). Fig. 3 shows as illustration the variation of the dielectric permittivity (ε_r) with

Table 1. Lattice parameters, tetragonality and unit cell volume (V) of BCYTx.

x (%)	a (A^0)	c (A^0)	(c/a)	V ($A^{0\,3}$)
0	4.0096	4.0114	1.00044	64.4908
1	4.0089	4.0100	1.00027	64.4458
3	4.0085	4.0093	1.00019	64.4217
5	4.0078	4.0085	1.00017	64.3863
7	4.0074	4.0080	1.00014	64.3655
9	4.0396	4.0400	1.00009	65.9262

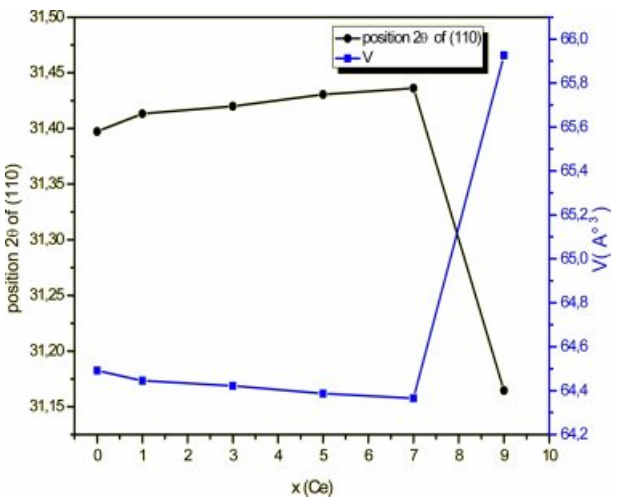

Fig. 2. Position of the peak (110) and unit cell volume of BCYTx samples as functions of x.

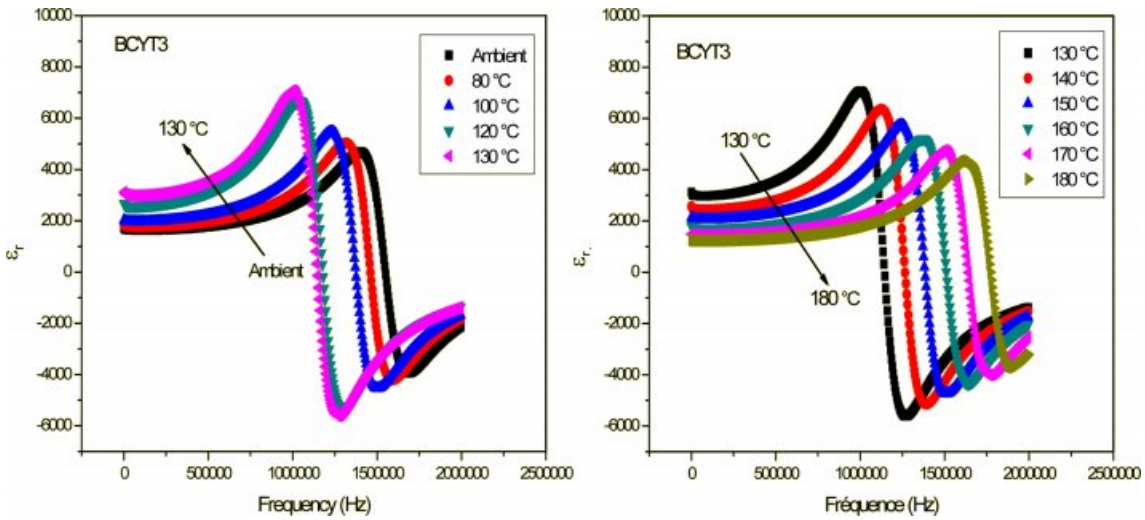

Fig. 3. Variation of dielectric permittivity with frequency of BCYT3 sintered at 1200 °C for 6 h.

frequency of the BCYT3 sample at different temperatures.

The different piezoelectric constants can be expressed as follows.

The planar electromechanical coupling factor K_p:

$$K_p^2 = \frac{\eta^2 - (1-\alpha^{E^2})}{2(1+\alpha^E)} * \frac{f_a^2 - f_r^2}{f_a^2} = 1.255 * \frac{f_a^2 - f_r^2}{f_a^2} \quad (1)$$

The Young Module E:

$$E = \left[\frac{\pi \phi f_r}{\eta}\right]^2 * (1-\alpha^{E^2}) * d \ (\mathrm{N/m^2}) \quad (2)$$

The piezoelectric constant of charge d:

$$d^A = K_p^A \sqrt{\frac{(1-\alpha^E)\varepsilon_r \varepsilon_0}{2E}} \ (C/N) \text{ at } 25\ ^\circ\mathrm{C} \quad (3)$$

The voltage constant g:

$$g^A = \frac{d^A}{\varepsilon_r \varepsilon_0}\left(m \cdot \frac{V}{N}\right) \text{ at } 25\ ^\circ\mathrm{C} \quad (4)$$

The calculation of the piezoelectric charge constant d^B and the voltage constant g^B at high temperatures was done using the following relations:

$$d^B = d^A \frac{K_p^B f_r^A}{K_p^A f_r^B} \sqrt{\frac{\varepsilon_r^A}{\varepsilon_r^B}}, \quad (5)$$

$$g^B = \frac{d^B}{\varepsilon_0 \varepsilon_r^B} \quad (6)$$

With:

Φ: Diameter of the sample (m)

α^E: The poisson coefficient (0.31 for ceramics)

η: The root of the Bessel equation (η = 2.05)

d: Density (Kg/m^3)

ε_0: is the permittivity of free space ($8.854*10^{-12}$ F/m)

ε_r: The relative permittivity

f_r: Resonance Frequency (Hz)

f_a: Anti-resonance frequency (Hz)

Tables 2, 3, 4 and 5 gather the values of the parameters f_r, f_a, ε_r, K_p, E, d^B and g^B for each temperature of the BCYTx samples (x = 0; 3; 7 and 9%). The planar electromechanical coupling factor, K_p, represents the ability of a ceramic to transform electrical energy into mechanical energy. The values that appear in Tables 2, 3 and 4 show an increasing behavior of this factor with temperature until a maximum around the temperature of the ferro-to-paraelectric transition, T_c, before it decreased (Fig. 4a). It was observed that incorporation of Ce^{3+} led to a decrease of T_c of the sample $BaTi_{0.97}Y_{0.03}O_3$. Sabina et al. [16] prepared $Ba_{1-x}Ce_xTiO_3$ ($0 \le x \le 0.04$) using the conventional solid state reaction method and has

Table 2. Values of the piezoelectric parameters of the sample BCYT0 heat treated at 1200 °C

T (°C)	f_r (MHz)	f_a (MHz)	ε_r	K_P	E (10^{12} N·m^{-2})	d^B (10^{-12} C·N^{-1})	g^B (10^{-3} V·m·N^{-1})
80	1.386000	1.706000	5173	0.65332	2.14155	56.1625	1.2262
100	1.356000	1.671000	5331	0.65478	2.04984	56.6743	1.2007
120	1.281000	1.591000	5721	0.66452	1.82936	58.7737	1.1603
140	0.886000	1.161000	9173	0.72396	0.87512	73.1108	0.9001
150	0.876000	1.151000	9862	0.72681	0.85547	71.5972	0.8199
160	0.916000	1.181000	9444	0.70726	0.93538	68.0869	0.8142
180	1.091000	1.361000	7874	0.66987	1.32694	59.2961	0.8505
200	1.341000	1.616000	6318	0.62526	2.00474	50.2686	0.8986
220	1.591000	1.876000	5189	0.59371	2.82190	44.3935	0.9662

Table 3. Values of the piezoelectric parameters of the sample BCYT3 heat treated at 1200 °C

T (°C)	f_r (MHz)	f_a (MHz)	ε_r	K_P	E (10^{12} N·m^{-2})	d^B (10^{-12} C·N^{-1})	g^B (10^{-3} V·m·N^{-1})
80	1.316000	1.596000	5037	0.63394	2.68709	44.6562	1.0013
100	1.231000	1.501000	5480	0.64114	2.35119	46.2887	0.9540
120	1.041000	1.301000	6688	0.67206	1.68141	51.9381	0.8771
130	1.001000	1.271000	7069	0.69048	1.55467	53.9771	0.8624
140	1.126000	1.391000	6360	0.65788	1.96720	48.2006	0.8559
150	1.246000	1.511000	5754	0.63385	2.40883	44.1221	0.8660
160	1.371000	1.641000	5206	0.61576	2.91639	40.9537	0.8884
170	1.501000	1.771000	4742	0.59467	3.49569	37.8522	0.9015
180	1.631000	1.901000	4336	0.5756	4.12742	35.2609	0.9184

Table 4. Values of the piezoelectric parameters of the sample BCYT7 heat treated at 1200 °C

T (°C)	f_r (MHz)	f_a (MHz)	ε_r	K_P	E (10^{12} N·m^{-2})	d^B (10^{-12} C·N^{-1})	g^B (10^{-3} V·m·N^{-1})
80	1.051000	1.326000	6959	0.6832	1.63171	67.5690	1.0966
90	0.971000	1.236000	7837	0.69329	1.39276	69.9355	1.0078
110	1.011000	1.271000	7833	0.67906	1.50987	65.8067	0.9488
120	1.101000	1.361000	7232	0.65869	1.79065	61.0018	0.9526
130	1.236000	1.496000	6455	0.63125	2.25670	55.1208	0.9644
140	1.426000	1.691000	5580	0.60222	3.00383	49.0227	0.9922
150	1.526000	1.791000	5211	0.58655	3.43990	46.1712	1.0007
160	1.671000	1.936000	4736	0.56585	4.12467	42.6673	1.0175

Table 5. Values of the piezoelectric parameters of the sample BCYT9 heat treated at 1200 °C

T (°C)	f_r (MHz)	f_a (MHz)	ε_r	K_P	E (10^{12} N·m^{-2})	d^B (10^{-12} C·N^{-1})	g^B (10^{-3} V·m·N^{-1})
60	0.911000	1.181000	8373	0.71305	1.28959	83.0768	1.1206
80	1.001000	1.256000	8281	0.67679	1.55697	72.1600	0.9841
100	1.241000	1.501000	6734	0.63030	2.39308	60.1115	1.0081
120	1.441000	1.701000	5783	0.59538	3.22657	52.7680	1.0305
140	1.696000	1.956000	4829	0.55820	4.46956	45.9997	1.0758

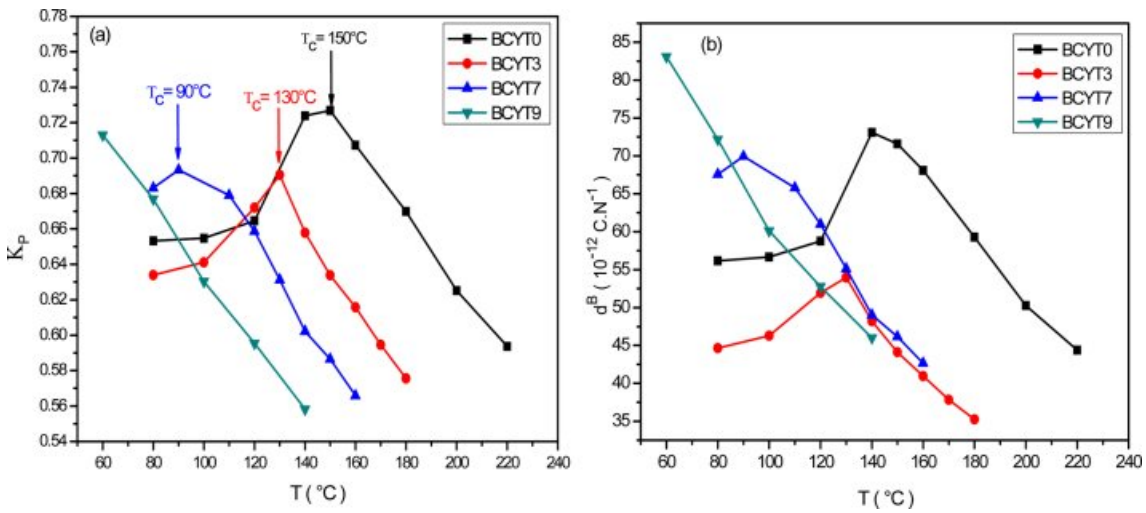

Fig. 4. (a) Thermal variations of the planar electromechanical coupling factor of BCYTx samples, (b) Thermal variations of the piezoelectric charge constant of BCYTx samples.

found that the T_c was decreased with increasing Ce content.

The piezoelectric charge coefficient d^B (Fig. 4b), has the same variation as K_p; this coefficient reached its maximum value around T_c and then decreased. This decrease may be due to thermal agitation which is responsible of a disorder in the material.

We noticed that the piezoelectric voltage coefficient,

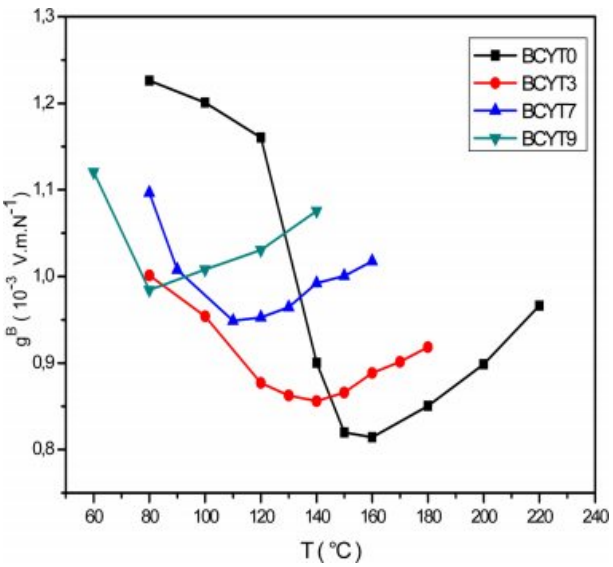

Fig. 5. Thermal variations of the voltage constant of BCYTx samples.

g^B, decreased first with increasing temperature and reached its minimum value around T_c and then increased (Fig. 5). It is clear that optimum values of the piezoelectric coefficients are all observed around T_c.

Table 6 compares the obtained values of the piezoelectric parameters for BCYTx samples with some of these constants collected from the literature. Incorporation of Ce did not improve the piezoelectric constants, in particular the piezoelectric charge coefficient. Moreover, lower values of this parameter were recorded compared with those of Brajesh et al. [19] due probably to the presence of Yttrium in our samples.

Complex impedance and electrical modulus studies

The electrical properties of a material are normally determined from the dielectric data with the help of the following relations:

Complex permittivity: $\varepsilon^* = \varepsilon' - i\varepsilon''$ (7)

Dielectric loss: $\tan\delta = \frac{\varepsilon''}{\varepsilon'} = -\frac{z'}{z''} = \frac{M''}{M'}$ (8)

Complex impedance:

$$Z^* = Z' + iZ'' = \frac{\varepsilon''}{C_0\omega(\varepsilon'^2+\varepsilon''^2)} + \frac{(-\varepsilon')}{C_0\omega(\varepsilon'^2+\varepsilon''^2)} \quad (9)$$

Where $\omega = 2\pi f$ is the angular frequency, C_0 is the capacitance of the cell in vacuum, (ε', Z') and (ε'', Z'') are the real and imaginary components of permittivity and impedance, respectively.

Fig. 6(a) shows the frequency dependence of the real part Z' at different temperatures of the sample

Table 6. Values of the piezoelectric parameters compared with other studies.

Method of preparation	Ceramics		d^B (10^{-12} C·N^{-1})	g^B (10^{-3} V·m·N^{-1})	Reference
Sol gel	$(Ba_{1-x}Sr_x)TiO_3$	x=0.10	98.02649	1.13448	El Ghandouri et al. [21]
Conventional solid state route	$Ba(Ti_{1-x}Ce_x)O_3$	x=0.00	190	- - - - - -	Brajesh et al. [19]
		x=0.02	254	- - - - - -	
Conventional solid state route	$Ba_{1+x}TiO_3$-0.04LiF	x=0.025	340	- - - - - -	Li-Feng Zhu et al. [22]
Sol gel	$(Ba_{1-x}Ce_x)(Ti_{(0.9775-x/4)}Y_{0.03})\ O_3$	x=0.00	71.5972	0.8199	Present work
		x=0.03	53.9771	0.8624	
		x=0.07	69.9355	1.0078	

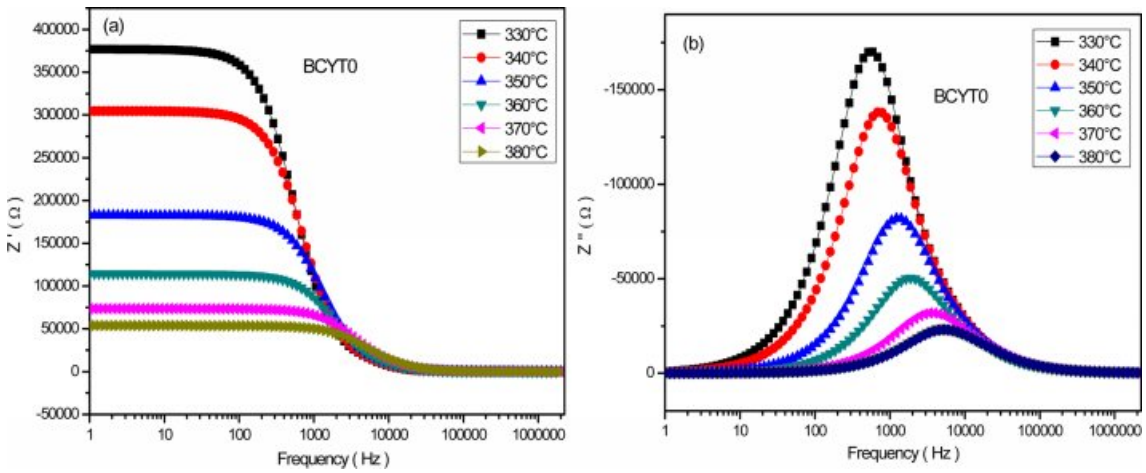

Fig. 6. (a) Variation of Z' as a function of the frequency for BCYT0 at various temperatures, (b) Variation of Z'' as a function of the frequency for BCYT0 at various temperatures.

$BaTi_{0.97}Y_{0.03}O_3$. This figure shows a decrease of Z' in the low frequency interval with increasing temperature followed by a saturation in the high frequency region. This indicates the presence at low frequency of all types of polarisation mechanisms in the sample. Fig. 6(b) displays the frequency dependence of the imaginary part of Z" at different tempertures of the sample BCYT0, and shows first an increase of this parameter with frequency before reaching a maximum that shifts to the high frequency region with increasing temperature and then decreases to an almost quasi constant value. The broadening of the peaks indicates a possible distribution of relaxation times.

Fig. 7 displays the Nyquist diagram of BCYT0 at different temperatures, which consisted in half circles that are dominated by the grain boundaries resistance R_{gb}. Indeed, grain resistance (R_g) is very weak compared to that of the grain boundaries, as revealed by their values gathered in Table 7. The grain boundaries and grains effects were each modeled by a constant phase element parallel to a resistance.

El Ghandouri et al. [23] in their dielectric study of $Ba_{1-x}La_xTi_{(1-x/4)}O_3$ ($0 \leq x \leq 0.4$) samples obtained similar results pointing out the strong effect of grain boundaries on the conduction mechanism in these compounds.

By adjusting our experimental data with the help of the equivalent circuit of Fig. 8, values of the capacitance and the resistance of grains (C_g, R_g) and grain boundaries (C_{gb}, R_{gb}) were determined using Z view software and given in Table 7.

The complex electrical modulus (M*) is defined as a function of the complex dielectric permittivity (ε*) by the following relation:

$$M^* = M' + iM'' = \frac{\varepsilon'}{\varepsilon'^2 + \varepsilon''^2} + \frac{\varepsilon''}{\varepsilon'^2 + \varepsilon''^2} \quad (10)$$

Where M' and M" are the real and imaginary parts of

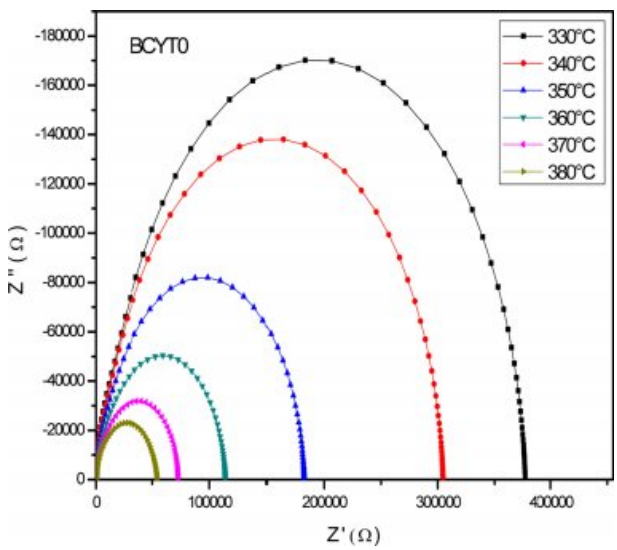

Fig. 7. Impedance curves of the sample BCYT0 at various temperatures.

Fig. 8. Equivalent circuits used for fitting the experimental data of the sample BCYT0.

Table 7. The resistance and capacitance of grain and grain boundary at various temperatures of the sample BCYT0.

T(°C)	C_g (nF)	R_g (KΩ)	C_{gb} (nF)	R_{gb} (KΩ)
330	0.6253	12.075	1.1498	364.91
340	0.8539	10.15	1.0830	294.65
350	0.9979	8.034	1.1040	187.88
360	0.9913	6.621	1.1650	107.67
370	0.9045	4.552	1.2620	68.929
380	0.8620	3.987	1.3720	49.727

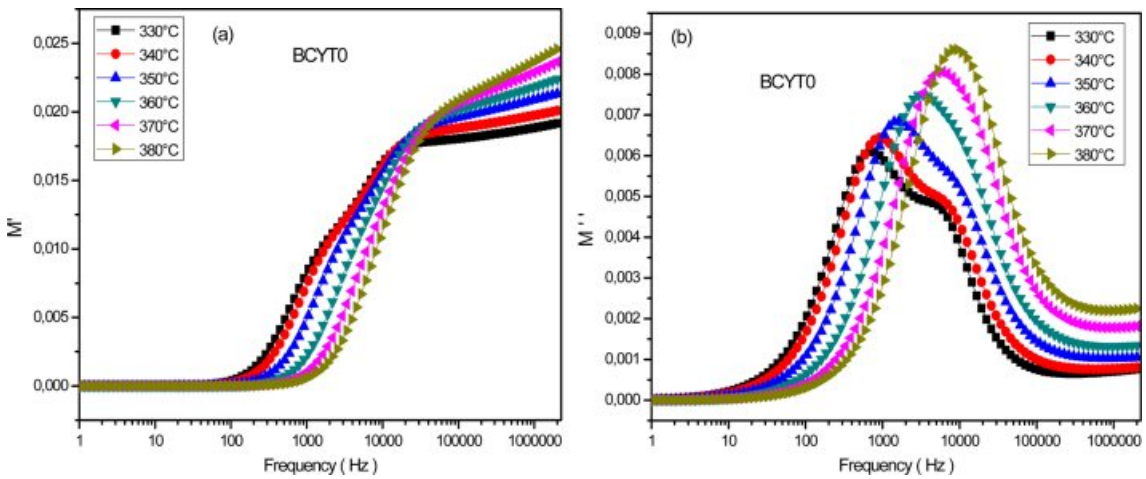

Fig. 9. (a) Variation of M' as a function of the frequency for BCYT0 at various temperatures, (b) Variation of M" as a function of the frequency for BCYT0 at various temperatures.

the complex electric modulus M*, respectively.

Fig. 9(a) displays the frequency dependence of the real part of M' determined at different temperatures for the sample BCYT0. This figure showed a very weak value of M' at low frequencies followed by a dispersion with increasing frequency and reached a finite limit that increased with increasing temperature. The latter behavior may be due to the mobility at short distances of charge carriers [24]. Fig. 9(b) displays the frequency dependence of the imaginary part M" at different temperatures of the sample BCYT0. This figure showed that M" increased with increasing frequency, passed through a maximum which moved towards high frequency region and which magnitude increased with temperature. This behavior suggests a thermal activated relaxation process [24].

Conclusion

Ce-doped $BaTi_{0.97}Y_{0.03}O_3$ ceramics were successfully prepared and their piezoelectric and impedance constants determined from resonance and antiresonance values given by dielectric measurements. Structural analysis showed that Ce^{3+} ions occupied Ba sites until x = 0.07 and then incorporated Ti sites indicating that the concentration 0.07 represents a solubility limit in $BaTi_{0.97}Y_{0.03}O_3$. It was also observed that in the presence of Yttrium and in the range of concentrations in Ce studied, the mechanism of conduction is strongly affected and dominated by grain boundaries. Moreover, the incorporation of Ce did not enhance the piezoelectric parameters compared to some published ones. More work is needed to clarify the role of Y atoms and site occupation of Ce atoms in inhibiting the piezoelectric constants.

References

1. L. H. Parker and A. F. Tasch, IEEE Circuits Devices Mag 6[1] (1990) 17-26.
2. K. K. Deb, Ferroelectrics 82[1] (1998) 45-53.
3. L.A. Thomas, Ferroelectrics 3[1] (1972) 231-238.
4. D.Y. Lu, Y. Yue, and X.Y. Sun, J. Alloys Compd. 586 (2014) 136-141.
5. E.P. Pevtsov, E.G. Elkin, and M.A. Pospelova, Int .Soc. Opt. Am. 3200 (1997) 179-182.
6. R. Guo, L.E. Cross, S.E. Park, B. Noheda, D.E. Cox, and G. Shirane, Phys. Rev. Lett. 84[23] (2000) 5423-5426.
7. W.F. Liu and X.B. Ren, Phys. Rev. Lett. 103[25] (2009) 257602.
8. Y. Feng, W.L. Li, D. Xu, Y.-.L. Qiao, Y. Yu, Y. Zhao, and W.-D. Fei, ACS Appl. Mater Interf. 8[14] (2016) 9231-9241.
9. S.J. Zhang, R.E. Eitel, C.A. Randall, T.R. Shrout, and E.F. Alberta, Appl. Phys. Lett. 86[26] (2005) 262904.
10. S. Lee, C.A. Randall, and Z.K. Liu, J. Am. Ceram Soc. 91[6] (2008) 1753-1761.
11. A.A. Yaremchenko, S. Populoh, S.G. Patricio, J. Macias, P. Thiel, D.P. Fagg, A. Weidenkaff, J.R. Frade, and A.V. Kovalevsky, Chem. Mat. 27[14] (2015) 4995-5006.
12. S.H. Ding, T.X. Song, and G.B. Liu, Ferroelectrics 445[1] (2013) 26-31.
13. D. Xu, W.L. Li, L.D. Wang, W. Wang, W.P. Cao, and W.D. Fei, Acta Mater 79 (Supplement C) (2014) 84-92.
14. Y. Feng, W.L. Li, D. Xu, and W.D. Fei, Ferroelectrics 489[1] (2015) 156-163.
15. F.A. Ismail, R.A.M. Osman, and M.S. Idris, AIP Conference Proceedings 1756 (2016) 090005.
16. S. Yasmim, S. Choudhury, M.A. Hakim, A.H. Bhuiyan, and M. J. Rahman, J. Mater. Sci. Technol. 27[8] (2011) 759-763.
17. F. Es-saddik, K. Limame, S. Sayouri, and T. Lamcharfi, J. Mater. Sci.: Mater. Electron. 30[2] (2019) 1821-1831.
18. Y. Tsur and C.A. Randall, Jpn. J. Appl. Phys. 40[1] (2001) 255-258.
19. K. Brajesh, A.K. Kalyani, and R. Ranjan. Appl. Phys. Lett. 106[1] (2015) 012907.
20. B. Jaffe, S. Roth, and S. Marzullo, J. Res. Natl. Bur. Stand. 55[5] (1955) 239-254.
21. A. El Ghandouri, S. Sayouri, T. Lamcharfi, and L. Hajji, J. Ceram. Process. Res. 19[2] (2018) 154-170.
22. L. Zhu, B. Zhang, and W. Yang, Mater. Res. Bull.52 (2014) 158-161.
23. A. El Ghandouri, S. Sayouri, T. Lamcharfi, and A. Elbasset, J. Adv. Dielect. 9[3] (2019) 1950026.
24. B.K. Singh and B. Kumar, Cryst. Res. Technol. 45[10] (2010) 1003-1011.